REVISION 1

Recognizing sulfate and phosphate complexes chemisorbed onto nanophase weathering products on Mars using *in-situ* and remote observations

Elizabeth B. Rampe[1], Richard V. Morris[2], P. Douglas Archer, Jr.[3], David G. Agresti[4], and Douglas W. Ming[2]

[1]Aerodyne Industries, Jacobs JETS Contract at NASA Johnson Space Center, 2101 Nasa Pkwy, Mail Code XI3, Houston, TX 77058, U.S.A. Email: elizabeth.b.rampe@nasa.gov

[2]NASA Johnson Space Center, Houston, TX 77058, U.S.A.

[3]Jacobs, NASA Johnson Space Center, Houston, TX 77058, U.S.A.

[4]University of Alabama at Birmingham, Department of Physics, Birmingham, AL 35294, U.S.A.

Abstract

Orbital and *in-situ* data from the surface of Mars indicate that nanophase weathering products are important constituents of martian rocks and soils. Nanophase minerals have the capacity to chemisorb anions like sulfate and phosphate onto their surfaces, but it is not known whether chemisorption is an important or even detectable process via orbital and *in-situ* observations. The detection of chemisorbed sulfate and phosphate anions on nanophase minerals would constrain the speciation of these anions and past aqueous environmental conditions. Here, we synthesized two nanophase weathering products that are common in terrestrial volcanic soils and have been identified on the martian surface: allophane and nanophase ferric oxide as represented by ferrihydrite. We specifically adsorbed sulfate and phosphate separately onto the nanophase mineral surfaces (4.5 wt% and 1.6 wt% SO_4^{2-} and 6.7 wt% and 8.9 wt% PO_4^{3-} on allophane and ferrihydrite, respectively) and analyzed the untreated and chemisorbed materials using instruments similar to those on orbital and landed Mars missions (including X-ray diffraction, evolved gas analysis, Mössbauer spectroscopy, and VNIR and thermal-IR spectroscopy). Evolved gas analysis is the optimum method to detect chemisorbed sulfate, with $SO_{2(g)}$ being released at >900 °C for allophane and 400-800 °C for ferrihydrite. Chemisorbed sulfate and phosphate anions affect the thermal-IR spectra of allophane and ferrihydrite in the S-O and P-O stretching region when present in abundances of only a few weight percent; S-O and P-O stretching bands are apparent as short-wavelength shoulders on Si-O stretching bands. Sulfate and phosphate anions chemisorbed to allophane have small but measurable effects on the position of the OH-H_2O bands at 1.4 and 1.9 μm in near-IR spectra. Chemisorbed sulfate and phosphate anions did not affect the X-ray diffraction patterns, Mössbauer spectra, and visible/near-IR spectra of ferrihydrite. These data suggest that sulfate chemisorbed onto the

surfaces of nanophase minerals can be detected with the Sample Analysis at Mars (SAM) instrument on the Mars Science Laboratory *Curiosity* rover, and subtle signatures of chemisorbed sulfate and phosphate may be detectable by IR spectrometers on landed missions. The combined use of SAM, the Chemistry and Mineralogy (CheMin) instrument, and the Alpha Particle X-ray Spectrometer (APXS) on *Curiosity* allows for the most detailed characterization to date of nanophase minerals in martian rocks and soils and the potential presence of chemisorbed anionic complexes.

Keywords: Mars, nanophase minerals, chemisorption, spectroscopy, evolved gas analysis, X-ray diffraction

Introduction

Precise characterization of chemical weathering products on Mars is important for understanding past and present aqueous environments and for interpreting the habitability of the martian surface. Nanophase weathering products (npWP) are short-range order, nanometer-scale materials and have been detected on the martian surface via *in-situ* and orbital measurements. *In-situ* measurements by the instrument payloads onboard the Mars Pathfinder rover and the Mars Exploration Rovers (MER) are consistent with the presence of nanophase Fe-oxides/oxyhydroxides in the rocks, soils, and dust, including any combination of superparamagnetic hematite and goethite, iddingsite, hisingerite, schwertmannite, akaganeite, ferrihydrite, and a poorly crystalline ferric iron phase associated with unknown amounts of H_2O and OH that is found in terrestrial palagonitic tephra (Morris et al. 2000; Morris et al. 2006a, 2006b). These phases can be present in abundances up to ~66 wt% in rocks and soils at Gusev crater (Ming et al. 2006). Phase models of APXS chemical data from MER in Meridiani and Gusev suggest that allophane, a poorly crystalline aluminosilicate ($Al_2O_3 \bullet xSiO_2 \bullet yH_2O$, x =

70 0.8-2, $y \geq 2.5$), is present in some weathered rocks in abundances of up to ~70 wt% (Clark et al.
71 2005; Ming et al. 2006). Thermal-infrared spectral models of regional Thermal Emission
72 Spectrometer (TES) data suggest that allophane occurs in ~10 vol% abundances over large areas,
73 including Northern Acidalia, Meridiani Planum, Solis Planum, and Aonium-Phrixi (Rampe et al.
74 2012). X-ray diffraction data measured by the Chemistry and Mineralogy (CheMin) instrument
75 on the Mars Science Laboratory (MSL) *Curiosity* rover show that amorphous phases are
76 important portions of rocks and soils at Gale crater. Models of CheMin data from the Rocknest
77 sand shadow and the Sheepbed mudstone determined that both samples are composed of ~30
78 wt% amorphous phases (Bish et al. 2013; Blake et al. 2013; Vaniman et al. 2014), and
79 calculations of the composition of the amorphous component suggest these samples may be
80 composed of 40-50 wt% amorphous phases (e.g., Dehouck et al. 2014; Morris et al. 2015a).
81 The types of npWP present on the martian surface inform us about the chemical
82 weathering environment. Allophane, a precursor to high-SiO_2 and high-Al_2O_3 clay minerals, is
83 composed of hollow spheres 3-5 nm in diameter. The sphere wall is made up of a rolled
84 octahedral Al-OH sheet with pores, and low-Si allophane has isolated orthosilicate tetrahedra
85 bonded to the octahedral sheet through three Al-O-Si links, with one Si-O-H group pointing
86 inwards. The orthosilicate tetrahedra display some polymerization in high-Si allophane (e.g.,
87 Parfitt and Hemni 1980; Parfitt 1990). Allophane and imogolite, a paracrystalline hydrated
88 aluminosilicate, most commonly form from chemical weathering of volcanic glass at pH 5-7
89 (Wada 1987). Nanophase iron-oxides/oxyhydroxides (npOx) form when ferrous iron (Fe^{2+}) is
90 released into solution (usually by dissolution of Fe-bearing silicates like olivine, pyroxene, and
91 volcanic glass) and oxidized to form ferric iron (Fe^{3+}). Ferric iron immediately hydrolyzes in the
92 presence of H_2O because of its high affinity for OH^- and polymerizes with further hydrolysis,

thus forming Fe-oxides/oxyhydroxides (Schwertmann and Taylor 1989). Ferrihydrite ($5Fe_2O_3 \cdot 9H_2O$) forms by aqueous alteration in solutions with pH >3 and is composed of spherical particles 3-7 nm in diameter. Under oxidizing conditions, hydration of Fe-bearing glass can result in precipitation of npOx within the glassy matrix. An example is the alteration of basaltic glass to npOx (with an unknown hydration and hydroxylation state) and other alteration products including allophane and halloysite (Morris et al. 1993, 2001).

NpWP are important constituents of weathered basalts and volcanic soils on Earth because they influence physico-chemical properties such as ion adsorption and solute transport. The characteristics of nanophase weathering products that allow them to control these properties are their surface structure and variable surface charge. When these materials are in aqueous fluids, the hydroxylated or hydrated nanophase mineral surface can be negatively or positively charged by desorption or adsorption of H^+, respectively (Schwertmann and Taylor 1989). The relative amounts of positively- and negatively-charged sites on the mineral surface are dependent on the pH of the solution, where a decrease in pH favors more positively-charged surfaces as more H^+ is available in solution. Because their surface charges are variable, npWP can adsorb cations and/or anions, which affects the transportation of ions in solution. Ions can be adsorbed by non-specific adsorption (ions retained through electrostatic forces) and specific adsorption or chemisorption (ions retained through formation of covalent bonds) (Nanzyo et al. 1993). Sulfate and phosphate anions are specifically adsorbed onto nanophase Fe- and Si/Al-oxides in terrestrial soils, and this chemisorption affects the surface structure of the oxide particles (e.g., Kwon and Kubicki 2004; Ishiguro et al. 2006; Figure 1).

Although npWP have been identified on Mars through remote and *in-situ* observations, it is not known if chemisorption has occurred on their surfaces. For example, npOx has been

identified at the MER landing sites with M□ssbauer spectroscopy, and SO_3 concentrations measured by the Alpha Particle X-ray Spectrometer (APXS) are correlated with npOx abundances (Morris et al. 2006a, 2006b). These data suggest that sulfur could be adsorbed onto the npOx surfaces, but the speciation of sulfur is unknown (e.g., it could instead be present in a separate iron sulfate phase like schwertmannite). Chemical data from APXS in Gusev show that rocks and soils can have up to ~5 wt% P_2O_5 and ~30 wt% SO_3 (Ming et al. 2006), but phase models of the mineralogy of martian rocks and soils assume that none of the phosphate or sulfate is chemisorbed onto weathering products. Calculations of the composition of the X-ray amorphous component of the Rocknest soil at Gale crater show abundances of ~2-3 wt% P_2O_5 and ~10-17 wt% SO_3 (Blake et al. 2013; Dehouck et al. 2014; Morris et al. 2015a), and the X-ray amorphous component in the Sheepbed mudstone has abundances of 2-3 wt% P_2O_5 and 0-11 wt% SO_3 (Vaniman et al. 2014; Dehouck et al. 2014; Morris et al. 2015a). Phosphate and sulfate could be chemisorbed onto the surfaces of nanophase minerals in these samples or present as discrete amorphous phases, such as amorphous sulfate salts (Morris et al. 2015b). The detection and quantification of chemisorbed ions onto weathering products would improve phase models from chemical data and help constrain the secondary mineralogy of the martian surface. Furthermore, the chemisorption of phosphate onto the surface of ferrihydrite can inhibit its transformation to a crystalline Fe-oxide (i.e., hematite or goethite) and generally favors its transformation to hematite over goethite (Gálvez et al. 1999), which may be relevant alteration reactions on Mars (e.g., Catling and Moore 2003; Chevrier et al. 2004).

Here, we report the characterization of chemisorbed phosphate and sulfate anions on synthetic ferrihydrite and allophane using laboratory instruments that have counterparts onboard the MER and MSL rovers; the Phoenix lander; and the Mars Global Surveyor (MGS), Mars

Reconnaissance Orbiter (MRO), and Mars Express (MEx) orbiting platforms. Our measurements include visible, near-IR spectroscopy (VNIR), M□ssbauer spectroscopy, thermal and evolved gas analysis (EGA), X-ray diffraction (XRD) analysis, and thermal-IR (TIR) emission spectroscopy.

Materials and Methods

Nanophase mineral syntheses and ion chemisorption procedures

Two batches of allophane were synthesized from aluminum chloride and sodium orthosilicate solutions using methods adapted from Wada et al. (1979) and Ohashi et al. (2002) to obtain allophane samples with Si/Al molar ratios between 0.5 and 1. Syntheses produced allophane samples having Si/Al molar ratios of 0.7 and 0.9 (determined by atomic absorption spectroscopy). Two-line ferrihydrite was synthesized according to Schwertmann and Cornell (2000). Allophane and ferrihydrite samples were freeze dried, rather than air dried, to achieve very small particle cluster sizes and high surface-to-volume ratios to produce a large surface area for chemisorption.

Sulfate and phosphate chemisorption procedures were adapted from previously published procedures. For allophane, 15 mM solutions of SO_4^{2-} and PO_4^{3-} were prepared using K_2SO_4 and K_2HPO_4, respectively, and the pH of each solution was adjusted to 5.5 with HCl and KOH (after Jara et al. 2006 and Cichota et al. 2007). We selected pH 5.5 for the allophane chemisorption experiments because phosphate is rapidly and strongly chemisorbed to allophane at pH 5-6 (Parfitt 1990). For ferrihydrite, 15 mM solutions of SO_4^{2-} and PO_4^{3-} were prepared using K_2SO_4 and Na_2HPO_4, respectively, and the pH of the solution was adjusted to 4 with HCl and NaOH (after Willett et al. 1988). We selected pH 4 for the ferrihydrite chemisorption experiments to ensure high surface coverage of phosphate ligands (Willett et al. 1988). The ionic strength of

each solution was maintained using KCl as a background electrolyte (0.1 mol/L). The final volume of each solution was 100 mL, and 10 mL of each solution was reserved for ion chromatography to obtain the initial SO_4^{2-} and PO_4^{3-} concentrations. Approximately 1.2 g of either allophane or ferrihydrite was added to the SO_4^{2-} and PO_4^{3-} solutions. An aliquot of each supernatant was reserved for IC after continuously stirring the solutions for 24 hours to determine (by difference) the amount of SO_4^{2-} and PO_4^{3-} that had adsorbed on npWP surfaces. The materials were then centrifuged and washed with milliQ water to remove any remaining salts and non-specifically adsorbed ions and oven dried in air at 50 °C. Each chemisorption experiment was performed once. The Si/Al ratio of allophane affects the extent of chemisorption, where there is greater chemisorption with decreasing Si/Al ratio (Parfitt 1990) because silanol groups bond to aluminol groups, thus diminishing the sites to which ligands like sulfate and phosphate can bond (Elsheikh et al. 2009). Phosphate was chemisorbed to allophane with an Si/Al ratio of 0.7, whereas sulfate was chemisorbed to allophane with an Si/Al ratio of 0.9. As such, phosphate likely chemisorbed to a greater extent than would have occurred if phosphate was chemisorbed to allophane with Si/Al = 0.9.

The concentrations of sulfate and phosphate chemisorbed onto allophane and ferrihydrite were quantified by ion chromatography (IC) at NASA Johnson Space Center (JSC) using a Dionex ICS-2000 ion chromatograph. IC analyses of the starting solutions and the solutions after stirring revealed that the allophane had 4.5 wt% chemisorbed SO_4 and 6.7 wt% chemisorbed PO_4 (3.7% SO_3 and 10.0% P_2O_5) and the ferrihydrite had 1.6 wt% chemisorbed SO_4 and 8.9 wt% chemisorbed PO_4 (1.3% SO_3 and 13.3% P_2O_5). These values do not necessarily represent the maximum amount of sulfate and phosphate that can be chemisorbed onto allophane and

ferrihydrite; greater amounts of sulfate can be chemisorbed on allophane at pH 4.5 than pH 5.5 (Jara et al. 2006).

Previous studies on phosphate and sulfate chemisorbed ferrihydrite and allophane suggest that these anions formed bidentate surface complexes (Figures 1b and 1c) on the positively charged allophane and npOx surfaces (e.g., Rajan 1979; Kwon and Kubicki 2004; Khare et al. 2007; Antelo et al. 2010; Zhu et al. 2014). NpWP surfaces are positively charged in aqueous solutions with pH less than the point of zero charge (PZC) of the nanophase mineral. The PZC of allophane and ferrihydrite are ~6.5 and ~8.0, respectively (e.g., Su and Harsh 1993; Antelo et al. 2010). Because we performed our sulfate and phosphate chemisorption experiments at pH 4 and 5.5 for ferrihydrite and allophane, respectively (i.e., below the PZC of both npWP), we infer that the structure of the surface complexes is bidentate. Furthermore, greater concentrations of anionic complexes will chemisorb to positively charged surfaces than to negatively charged surfaces, so performing these experiments below the PZC increases the concentration of surface complexes.

Instrumental methods

Transmission electron microscopy was performed using the JEOL 2500SE 200 kV field-emission scanning-TEM at JSC equipped with a thin window energy-dispersive X-ray (EDX) spectrometer. These measurements were made to ensure samples were amorphous (i.e., no spots indicating crystallinity in electron diffraction patterns) and to assess structural and compositional homogeneity in the samples (e.g., no discrete sulfate or phosphate particles).

XRD analyses were made on a Panalytical X-Pert Pro MPD instrument at JSC. Patterns were measured from 2-80 °2θ with Cu-Kα or Co-Kα radiation on a traditional spinner stage. The

206 2θ range for the MSL XRD instrument (CheMin) is 5 to 50 °2θ (Co-Kα radiation) (Blake et al.
207 2012).

208 Thermal and evolved gas analyses were done at JSC using a Netzsch STA 449 F1 Jupiter
209 simultaneous thermogravimetry/differential scanning calorimetry analyzer coupled to a Pfieffer
210 ThermoStar GSD 320 quadrupole mass spectrometer. Samples were heated from 30 to 1150 °C
211 at 35 °C/minute under conditions similar to those on the MSL EGA instrument, Sample Analysis
212 at Mars (SAM): 30 mbar He and 20 sccm flow rate (Mahaffy et al. 2012). The relevant evolved
213 gases (e.g., H_2O, SO_2) were measured by the mass spectrometer and recorded as a function of
214 temperature.

215 Iron M□ssbauer spectroscopy of the untreated and chemisorbed ferrihydrite (our
216 synthetic allophane has no Fe) was performed at JSC at room temperature using a MIMOS
217 (MIniaturized MOssbauer Spectrometer) II instrument (EPSI, Inc.). The instrument is a
218 backscatter M□ssbauer spectrometer with a ^{57}Co source and is the laboratory equivalent of the
219 flight M□ssbauer spectrometers on the MER rovers (Klingelh□fer et al. 2003), permitting
220 spectra collected here to be directly compared to MER M□ssbauer spectra. Velocity calibrations
221 and least-squares fit of the spectra were done with the computer program MERView and
222 MERFit, respectively (Agresti et al. 2006; Agresti and Gerakines 2009). All spectra were fit with
223 one-, two-, and three-doublet models with peak areas and widths for each doublet constrained to
224 be the same. The M□ssbauer parameters derived from the fits are the center shift (CS),
225 quadrupole splitting (QS), full width at half-maximum peak intensity (W), and doublet relative
226 area (A).

227 VNIR reflectance spectra were measured at JSC with Analytical Spectral Devices
228 FieldSpec3 fiber-optic based spectrometers from 350 to 2500 nm relative to a Spectralon

229 standard and converted to absolute reflectance. Measurements were made in air under ambient
230 temperature and humidity conditions and within a glove box purged with dry-N_2 gas (<110 ppm_v
231 H_2O). The H_2O_v abundance in the glove box is similar to that experienced on the martian surface
232 (e.g., Martín-Torres et al. 2015).

233 Spectral measurements within the glove box were made sequentially at 25-35 °C after
234 prolonged (~2-3 weeks) desiccation at 25-35 °C (room temperature), then after heating to 110 °C
235 and 220 °C on a hot plate. Samples were exposed to higher temperatures when no spectral
236 changes were seen after at least 48 hours (i.e., no change in H_2O bands, indicating a stable
237 hydration state). Desiccating conditions removes adsorbed H_2O from the nanophase minerals,
238 permitting examination of their spectral signatures as might be encountered on Mars and
239 detected by orbiting MEx Observatoire pour la Minéralogie, l'Eau, les Glaces et l'Activité
240 (OMEGA) and MRO Compact Reconnaissance Spectrometer for Mars (CRISM) VNIR
241 instruments (Bibring et al. 2004; Murchie et al. 2007). We suggest desiccation at temperatures
242 above ambient is a reasonable surrogate for desiccation at lower temperatures over geologic
243 timescales on Mars.

244 Thermal-IR emission spectra of compressed pellets (as opposed to loose powders) of
245 untreated and chemisorbed npWP were collected at the Mars Space Flight Facility at Arizona
246 State University using a Nicolet Nexus 670 spectrometer configured to measure emitted energy
247 (Christensen and Harrison 1993; Ruff et al. 1997). Pellets were created by compressing ~0.1 g of
248 particulate material to ~70 MPa (uncorrected for friction) in a hydraulic press for three minutes
249 (Michalski et al. 2005). Pellets were 1 cm in diameter and a few mm thick, placed in copper
250 sample cups painted black so that they behave as a spectral blackbody, and heated to 80 °C
251 before and during the experiments to increase the signal-to-noise ratio. Spectra were scanned 270

252 times over the course of ~4 minutes, from 200-2000 cm^{-1} with 2 cm^{-1} spectral resolution.
253 Blackbodies at 70 °C and 100 °C were measured to calibrate raw data to radiance (Christensen
254 and Harrison 1993). Heating likely caused partial dehydration of the samples; however, spectral
255 bands from H_2O do not interfere with bands in ferrihydrite, allophane, sulfate, or phosphate over
256 the scanned range. Radiance spectra were transformed to emissivity spectra by normalizing to
257 the Planck curve corresponding to the sample temperature (Ruff et al. 1997).

258 **Results**

259 **Transmission Electron Microscopy**

260 Transmission electron photomicrographs show that the sulfate- and phosphate-
261 chemisorbed npWP samples lack long-range crystallographic order and are homogenous (Figure
262 2). Allophane samples are comprised of clusters of nm-scale particles up to a few microns in
263 diameter, and high-resolution images show a lack of lattice fringes (Figures 2a and c). Selected
264 area electron diffraction (SAED) patterns show two diffuse rings (Figure 2b), corresponding to d
265 spacings of ~2.2 and ~3.4 Å. TEM of chemisorbed allophane samples show that they are
266 morphologically and structurally similar to previous studies of natural and synthetic allophane
267 (e.g., Wada 1989; Ohashi et al. 2002; Rampe et al. 2012). Ferrihydrite samples are similarly
268 comprised of clusters of nm-scale spherules (Figure 2d), and high-resolution TEM show some
269 small areas with lattice fringes (Figure 2f), showing areas of incipient crystallinity. SAED
270 patterns show two bright rings (Figures 2e), corresponding to d spacings of ~1.5 and 2.6 Å. TEM
271 of chemisorbed ferrihydrite samples are morphologically and structurally similar to previous
272 studies of natural and synthetic ferrihydrite (e.g., Schwertmann and Taylor 1989; Janney et al.
273 2000). TEM confirms that neither the chemisorbed allophane nor the chemisorbed ferrihydrite
274 contain discrete sulfate or phosphate phases.

X-Ray Diffraction

The broad XRD peaks with low intensities for untreated synthetic allophane and ferrihydrite demonstrate that these materials lack long-range crystallographic order. The peaks for allophane occur at 1.4, 2.2, and 3.4 Å (Figure 3a), consistent with previous XRD studies of natural and synthetic allophane (Wada 1989) and the rings measured in TEM-SAED patterns (Figure 2b). The XRD peak at 1.4 Å was not observed in TEM-SAED because it is very weak. The allophane pattern also displays a low-angle peak at ~24 Å, which has been attributed to diffraction off of closely packed spheres of allophane (van der Gaast et al. 1985). Previous studies of natural and synthetic allophane and imogolite have noted that this peak becomes more intense with dehydration (van der Gaast et al. 1985; Bishop et al. 2013) because as adsorbed water is removed, the spherules become more tightly packed. This phenomenon occurs in chemisorbed allophane because the chemisorption of ions to the allophane surface results in the removal of H_2O adsorbed to the surface (Figure 1). The peaks for two-line ferrihydrite occur at 1.5 and 2.6 Å (Figure 3b), consistent with previous XRD studies of natural and synthetic two-line ferrihydrite (e.g., Schwertmann and Cornell 2000; Bishop and Murad 2002) and the rings measured in TEM-SAED patterns (Figure 2e). Patterns from both npWP show a rise in intensity at low angles. The chemisorption of sulfate and phosphate onto allophane and ferrihydrite does not affect the position of the XRD peaks and generally does not affect the peak intensities (Figure 3). The only difference induced by the chemisorption of sulfate or phosphate is the intensity of the low-angle allophane peak at ~24 Å; this peak becomes more pronounced with the chemisorption of sulfate or phosphate and desorption of H_2O.

Thermal and Evolved Gas Analysis

297 Evolved gas analyses of the untreated samples show intense releases of gas with
298 mass/charge (m/z) equal to 18 (i.e., H_2O). EGA traces of m/z 18 from untreated allophane show
299 two, broad low-temperature releases followed by a steady decrease in the amount of H_2O
300 released with increasing temperature. The low temperature release occurs from ~50-400 °C, with
301 peak releases at ~120 and 275 °C (Figure 4a). These peaks relate to the removal of adsorbed and
302 structural H_2O, respectively (Borchardt 1989; Wada 1989). EGA traces of m/z 18 from untreated
303 ferrihydrite show one broad temperature release from ~50-350 °C with a maximum at ~120 °C
304 (Figure 4b). This broad release in the EGA data is from the loss of adsorbed and structural H_2O
305 and structural OH in ferrihydrite as it transforms to hematite (Schwertmann and Cornell 2000).
306 EGA data of m/z 18 from sulfate- and phosphate-chemisorbed allophane are similar to
307 the untreated allophane. The m/z 18 EGA data from sulfate- and phosphate-chemisorbed
308 ferrihydrite, however, differ from the untreated ferrihydrite data because a sharp release is
309 present at a peak temperature of 440 °C (Figure 4b). The temperature of this release corresponds
310 to the temperature at which ferrihydrite completely transforms to hematite, and this transition is
311 visible in the corresponding differential scanning calorimetry data (data not shown). The
312 presence of chemisorbed sulfate or phosphate on the surface of ferrihydrite thus inhibits the
313 transition to hematite until about 440 °C by preventing the aggregation and intimate contact of
314 ferrihydrite grains (Gálvez et al. 1999) so that the transition from ferrihydrite to hematite is not
315 gradual as it is in the untreated ferrihydrite sample, but instead is rapid with H_2O evolution over
316 a narrow temperature interval.
317 Evolved gas analyses of m/z 64 (i.e., SO_2) from sulfate-chemisorbed allophane show a
318 release with an onset temperature at ~900 °C and a peak release at ~960 °C (Figure 4). The
319 sulfate-chemisorbed ferrihydrite EGA data show releases of SO_2 at ~400, 490, and 700 °C.

Evolved gas analyses of phosphate-chemisorbed allophane and ferrihydrite do not show definitive evidence of the presence of phosphate because phosphate is not released as a gas below the maximum temperature of our experiments (1150 °C) (e.g., Frost et al. 2004; Gallini et al. 2005). Untreated ferrihydrite data display a m/z 30 release (NO) at ~200 °C from adsorbed nitrate (data not shown), which we interpret as a vestige of the synthesis from $Fe(NO_3)_3$ (Šubrt et al. 1992).

Mössbauer Spectroscopy

There were no detectable differences among the Mössbauer spectra for the untreated and chemisorbed ferrihydrite samples. As a representative example of the spectra from all samples, we show in Figure 5 the spectrum for sulfate-chemisorbed ferrihydrite with a 3-doublet fit. The values of the Mössbauer parameters are compiled in Table 1 for one- and three-doublet fits. The quality of the fit improves with additional doublets (decreasing values of χ^2), but the values of CS and QS for each doublet do not change within error for untreated and chemisorbed samples.

Visible Near-Infrared Spectroscopy

The VNIR reflectance spectrum of untreated allophane measured in lab air shows broad spectral bands with minima near 0.95, 1.4, 1.9, and 2.2 μm (Figure 6a). The first three minima result from overtones and combinations of the fundamental stretching and bending vibrations of the H_2O molecule and, for the 1.4 μm minimum only, overtones from the OH stretching vibration of the (Si,Al)OH functional group. The minimum near 2.2 μm is a combination of the bending and stretching vibration of the OH in the (Si,Al)OH functional group. Only the minimum near 1.9 μm requires the presence of the H_2O molecule (i.e., H-O-H stretching and bending vibrations). The band positions reported here are consistent with those previously reported for natural and synthetic allophane (e.g., Bishop et al. 2013). The band near 1.4 μm is a

343 doublet with minima near 1.38 and 1.40 μm (from the OH and H_2O overtone, respectively), as
344 was reported by Bishop et al. (2013), with greater contributions from the band at 1.38 μm as the
345 samples became more desiccated.

346 The VNIR reflectance spectrum of untreated ferrihydrite measured in lab air shows broad
347 spectral features with minima near 0.6, 1.0, 1.4, 1.9, and 2.3 μm (Figure 6b). The minimum near
348 1.9 μm results from overtones and combinations of the fundamental vibrations of the H_2O
349 molecule, as for allophane. The bands near 1.4 and 2.3 μm result from the Fe^{3+}-OH bending-
350 stretching combination vibrations, and the band near 1.4 μm also has a contribution from the
351 H_2O stretching overtone. Broad minima near 0.6 and 1.0 μm are from Fe^{3+} electronic transitions.
352 The band positions reported here are consistent with those previously reported for natural and
353 synthetic ferrihydrite (e.g., Bishop and Murad 2002).

354 With desiccation by exposure to dry $N_{2(g)}$ and with and without mild heating (Figure 6),
355 the amount of H_2O diminishes and is nearly absent from spectra for the allophane and
356 ferrihydrite samples heated to 220 ºC on the basis of the intensity of the 1.9 μm spectral feature.
357 For the 1.4 μm spectral feature, the corresponding changes with desiccation are decreasing
358 intensity and a shift of the band minimum to shorter wavelengths (1.43 to 1.38 μm and 1.43 to
359 1.40 μm for allophane and ferrihydrite, respectively). These intensity and position changes result
360 from decreasing contributions of the fundamental H_2O stretching overtone to the spectral feature
361 as the H_2O abundance decreases (on the basis of decreasing 1.9 μm band intensity) relative to the
362 contributions from (Si,Al)-OH and Fe-OH. Band minima of the 1.4 and 1.9 μm features are
363 similar for the untreated, sulfate-chemisorbed, and phosphate-chemisorbed ferrihydrite at each
364 stage of desiccation. However, these band minima are measurably different between the
365 untreated, sulfate-chemisorbed, and phosphate-chemisorbed allophane at each stage of

366 desiccation, such that the position of the bands of the untreated allophane are at the longest
367 wavelength and those of the phosphate-chemisorbed allophane are at the shortest wavelength
368 (Table 2).

369 For the 2.1 to 2.5 μm spectral region, the spectra of sulfate- and phosphate-chemisorbed
370 allophane samples exposed to the same temperature and humidity conditions are similar to their
371 untreated counterparts. It is unlikely that bands from vibrations of S-O and P-O bonds would be
372 detected with VNIR spectroscopy because these features would result from at least the fourth
373 overtone of such vibrations (Hunt et al. 1971).

374 The spectral features in the 2.1 to 2.5 μm region for the untreated and chemisorbed
375 ferrihydrite samples are much weaker in comparison to allophane (Figure 6). The strongest
376 feature is located at 2.30 μm (from Fe^{3+}-OH), and its intensity is not markedly dependent on the
377 extent of desiccation, although it broadens giving the appearance of an unresolved envelope of
378 more than one band. The phosphate-chemisorbed ferrihydrite spectra measured under desiccating
379 conditions have a weak band centered at 2.15 μm. We do not have sufficient information to
380 assign this band, but it occurs in the same spectral region as bands attributed to combinations of
381 OH stretching and bending vibrations (Bishop and Murad 2002).

382 The broad minima near 1.0 μm in the spectra of chemisorbed ferrihydrite have lower
383 reflectance than the minimum in the spectrum of untreated ferrihydrite. We hypothesize that the
384 chemisorption of spectrally neutral ligands (SO_4 and PO_4) caused a slight increase in albedo,
385 leading to the diminished reflectance near 1.0 μm.

386 **Thermal Emission Spectroscopy**

387 TIR spectra of compressed pellets of untreated allophane have broad bands at 950 cm^{-1}
388 from Si-O stretching vibrations, 550 cm^{-1} from Al-O-Si deformation vibrations, 420 cm^{-1} from

Si-O bending vibrations, and 340 cm^{-1} from Al-OH deformation vibrations (Figure 7a) (Rampe et al. 2012). The Si/Al ratio can affect the position of the Si-O stretching vibration, where the band is shifted to higher wavenumbers with increasing Si/Al ratio (e.g., Rampe et al. 2012); however, there were no differences between the TIR spectra of the two allophane samples we synthesized here. Sulfate- and phosphate-chemisorbed allophane have corresponding spectral features, but with a weak shoulder on the high frequency side of the Si-O stretching vibration at ~1050-1200 cm^{-1} and a shoulder on the high frequency side of the Al-O-Si deformation vibration at 600 cm^{-1}. The shoulder at 1050-1200 cm^{-1} is from S-O and P-O stretching and bending vibrations and the shoulder at 600 cm^{-1} is from S-O and P-O bending vibrations (Farmer 1974; Cloutis et al. 2006). TIR emission spectra of compressed pellets of all ferrihydrite samples have broad bands at 550 cm^{-1} and 300-450 cm^{-1} from Fe-O bending and Fe-O bending and stretching vibrations, respectively (Figure 7b) (Vempati et al. 1990). The untreated ferrihydrite spectrum is similar to transmission TIR spectra of synthetic ferrihydrite samples (Bishop and Murad 2002), including an unassigned V-shaped weak band near 1300 cm^{-1}. The TIR emission spectra of sulfate- and phosphate-chemisorbed ferrihydrite samples are similar to the spectrum of the untreated ferrihydrite from 350-950 cm^{-1}, but the chemisorbed ferrihydrite spectra have higher emissivity than the untreated ferrihydrite spectrum from ~1000-1350 cm^{-1}. This difference is a result of S-O and P-O stretching vibrations, which create Christiansen features (local maxima where the refractive index of the sample approaches that of the surrounding air (Conel 1969)) at ~1150 cm^{-1}. This feature is more apparent in the phosphate-chemisorbed ferrihydrite spectrum than the sulfate-chemisorbed ferrihydrite spectrum because more phosphate chemisorbed to the surface of ferrihydrite than sulfate (1.6 wt% SO_4 vs 8.9 wt% PO_4).

Implications for Martian Orbital and *In-Situ* Analyses

412 Our analyses of sulfate and phosphate chemisorbed onto allophane and ferrihydrite with
413 instruments that are laboratory counterparts to those on martian orbiter and landed missions
414 show that these instruments have different detection limits for chemisorbed anionic species on
415 the martian surface. EGA measurements, which were implemented as a part of the Phoenix
416 lander Thermal Evolved Gas Analyzer (TEGA) and the MSL SAM instrument packages
417 (Hoffman et al. 2008; Mahaffy et al. 2012), can distinguish allophane and ferrihydrite from their
418 forms chemisorbed with sulfate because the method directly detects evolved S-bearing species at
419 concentration levels expected in martian soils. Manifestations of chemisorbed sulfate and
420 phosphate anions are also observed in VNIR spectra of allophane and TIR spectra of both
421 allophane and ferrihydrite. VNIR spectra of ferrihydrite and XRD powder patterns and
422 Mössbauer spectra of both npWP show no apparent evidence for chemisorption at the
423 concentration levels of our experiments. We discuss these results in detail next, beginning with
424 EGA data.

425 Laboratory EGA of untreated allophane and ferrihydrite show that both phases have
426 similar, broad low-temperature H_2O releases with maxima near 120 ºC, and allophane has a
427 second maximum at ~275 ºC not seen in data from ferrihydrite. This additional peak provides
428 constraints for allophane versus ferrihydrite identification in martian samples using m/z 18 data
429 from SAM. Sulfate- or phosphate-chemisorbed ferrihydrite may be differentiated from anion-
430 free ferrihydrite in m/z 18 data with the observation of a release near 440 ºC from the rapid
431 transition from ferrihydrite to hematite.

432 With respect to SAM detection of chemisorbed sulfate or phosphate from S- or P-bearing
433 mass fragments, only sulfate detection is viable because phosphate does not undergo thermal
434 decomposition over SAM operating temperatures (ambient up to 1100 ºC; Mahaffy et al. 2012).

435 The m/z 64 EGA curves of sulfate-chemisorbed allophane and ferrihydrite show SO_2 releases
436 from >900 ºC and ~400-800 ºC, respectively, indicating that sulfate is indeed chemisorbed to the
437 surfaces of the npWP. Thus, samples must be heated to temperatures in excess of 900 ºC in order
438 to detect chemisorbed sulfate on allophane with SAM. To date, SAM thermal analyses have been
439 limited to a maximum of ~835 ºC (McAdam et al. 2014), permitting detection of chemisorbed
440 sulfate on ferrihydrite but not allophane. In addition, SO_2 evolution from some Mg- or Ca-sulfate
441 minerals may overwhelm the EGA signature of sulfate-adsorbed allophane if present in higher
442 abundances. For example, epsomite undergoes sulfate decomposition at 970 ºC under SAM-like
443 experimental conditions (Archer et al. 2013; Stern et al. 2013).

444 The m/z 64 EGA curve of sulfate-adsorbed ferrihydrite shows a series of SO_2 releases
445 with maxima at ~400, 490, and 700 °C (Figure 4b), and all three temperatures are within the
446 current operational range for SAM as discussed above. We attribute the higher ion current for the
447 m/z release for sulfate-chemisorbed allophane compared to ferrihydrite to the higher
448 concentration of chemisorbed sulfate to the former (4.5 wt% and 1.6 wt%, respectively, from IC
449 analyses). The presence of multiple m/z 64 releases might suggest the presence of multiple
450 sulfate phases. However, our TEM results show that the chemisorbed ferrihydrite samples are
451 homogenous and do not contain detectable separate sulfate phases.

452 To explain the m/z 64 releases at ~490 and 700 ºC in our experimental EGA data, we
453 hypothesize that the S-bearing gas species released at 400º C from the decomposition of sulfate
454 complexes chemisorbed to ferrihydrite surfaces reacted with the evolved H_2O vapor to form
455 secondary ferric sulfates during the experiment. Alternatively, the S-bearing gas species may
456 have reacted with the neo-formed hematite and chemisorbed to its surface. The subsequent
457 decomposition of these secondary products caused the SO_2 releases at ~490 and 700º C.

458 Furthermore, crystalline and amorphous ferric sulfates show SO_2 releases from ~500-800 ºC
459 (McAdam et al. 2014; Ming et al. 2014), consistent with the two higher-temperature m/z 64
460 releases in sulfate-chemisorbed ferrihydrite, and other common sulfate minerals (e.g., Ca-, Mg-,
461 and Al-sulfates) decompose at temperatures >500 ºC (e.g., Lombardi 1984; Archer et al. 2013;
462 Stern et al. 2013; McAdam et al. 2014; Ming et al. 2014). Thus, a m/z 64 release at 400 ºC in
463 SAM data would distinguish sulfate chemisorbed onto ferrihydrite from discrete crystalline and
464 amorphous ferric sulfates; however, this release has not been detected in SAM to date (McAdam
465 et al. 2014; Ming et al. 2014; McAdam et al. 2015). We hypothesize that similar reactions occur
466 during the heating of phosphate-chemisorbed ferrihydrite (i.e., formation of secondary ferric
467 phosphates or chemisorption of phosphate onto hematite); however, secondary ferric phosphates
468 would not be detected with SAM-EGA because their thermal decomposition temperatures
469 exceed the range of the experiments. In this case, the presence of a m/z 18 release at ~440 ºC but
470 the absence of a m/z 64 release at 400 ºC in SAM data may be evidence for chemisorbed
471 phosphate on ferrihydrite.

472 Rocks and soils in Gale crater measured to date are comprised of as little as 10-15 wt%
473 X-ray amorphous material, based on 2σ errors from XRD analyses (Bish et al. 2013; Blake et al.
474 2013; Vaniman et al. 2014), to as much as 50 wt%, based on chemical calculations (Morris et al.
475 2015a). Calculations of sulfate abundances in the amorphous component suggest it contains up to
476 ~10 wt% SO_3 (Morris et al. 2015a), which implies that up to ~5 wt% SO_3 in each bulk sample
477 can be attributed to the amorphous component (based on the assumption that 50 wt. % of the
478 sample is X-ray amorphous). Based on our laboratory EGA data, we expect to detect
479 chemisorbed sulfate with SAM if that speciation is present in abundances of at least 1.3 wt% SO_3
480 in association with a ferrihydrite-like material.

481 XRD patterns of chemisorbed allophane and ferrihydrite are very similar to the untreated
482 patterns, suggesting that chemisorption of sulfate and phosphate anions onto their surfaces does
483 not affect their internal structures within detection limits. The only observable difference was for
484 allophane where, at very low angles, the peak near 24 Å is more intense for the chemisorbed
485 allophane than for the untreated allophane. Although there is a difference in the intensity of this
486 low-angle peak between the untreated and chemisorbed allophane patterns, its location is outside
487 the angular range of the CheMin instrument (Blake et al. 2010). CheMin can distinguish between
488 untreated allophane and ferrihydrite on the basis of the positions of their broad diffraction peaks
489 which are within its angular range (Figure 3), but the instrument cannot distinguish between their
490 untreated and chemisorbed forms.

491 An important feature of the XRD patterns of allophane and ferrihydrite is the prominent
492 rise in intensity at low angles because CheMin patterns of all martian samples measured to date
493 display this feature. This increase in low-angle scattering intensity has been attributed to the
494 regular packing of nanophase particles (van der Gaast 1985; Bishop et al. 2013). However, the
495 low-angle rise is not present in patterns of all amorphous materials (e.g., igneous glasses do not
496 display this feature; Morris et al. 2015b). The increase in low-angle scattering intensity can be
497 used to determine the presence (but not the identity) of npWP from CheMin data.

498 Mössbauer spectra of chemisorbed ferrihydrite measured at room temperature show the
499 same doublet as the spectrum of untreated ferrihydrite. Mössbauer measurements of nanophase
500 iron oxides at low temperatures can reduce the effects of small particle size and isomorphous
501 substitution on the spectra so that they display a sextet instead of a doublet and nanophase iron
502 oxides can be distinguished from one another (e.g., Pollard et al. 1992). Two-line ferrihydrite, as
503 was studied here, displays a sextet in Mössbauer data when measured at extremely low

504 temperatures (i.e., 4.2 K; Pollard et al. 1992); however, ferrihydrite displays a doublet at 77 K
505 (Pollard et al. 1992). As such, we would not expect a sextet in Mössbauer data of ferrihydrite on
506 Mars, so the Mössbauer spectra collected here are similar to those that would be collected on the
507 martian surface. Furthermore, XRD patterns and TEM images indicate that crystalline structure
508 is not affected by chemisorption, so we suggest that Mössbauer measurements at very low
509 temperatures and modeling Mössbauer parameters from the subsequent sextets would not
510 provide further information about the effects of chemisorption on crystal structure.

511 The chemisorption of sulfate or phosphate onto allophane or ferrihydrite does not
512 introduce prominent spectral features that would readily permit VNIR spectral discrimination
513 from their counterparts without chemisorbed anions. This suggests that unequivocal detection of
514 chemisorbed sulfate and phosphate is unlikely from orbital VNIR instruments like OMEGA and
515 CRISM. However, the minima of the bands near 1.4 and 1.9 μm are at slightly shorter
516 wavelengths for the chemisorbed allophane samples than those for the untreated allophane
517 (Table 2). We suggest that this variation is the result of different relative H_2O abundances in the
518 samples. The band near 1.4 μm has a contribution from H_2O, and the band near 1.9 μm is from
519 H_2O. Chemisorption causes the removal of adsorbed H_2O, and as H_2O is removed from
520 allophane, the bands at 1.4 and 1.9 μm shift to shorter wavelengths (Bishop et al. 2013). More
521 phosphate is chemisorbed to allophane than sulfate in our samples, causing the 1.4 and 1.9 μm
522 band minima in the phosphate-chemisorbed allophane to be at shorter wavelengths than the
523 bands of sulfate-chemisorbed allophane. We speculate that this behavior is not seen in the NIR
524 spectra of the ferrihydrite samples because ferrihydrite has less H_2O than allophane (~14 vs. ~21
525 wt.%, respectively, for untreated samples as measured by thermal gravimetry) so that H_2O has a
526 markedly lower contribution to NIR spectra of ferrihydrite than allophane.

VNIR spectra of the untreated and chemisorbed ferrihydrite show the band near 520 nm shifts to longer wavelengths and the relative reflectance near 800 nm diminishes with heating (Figure 8), consistent with incipient bands for hematite at 630 and 860 nm (Morris et al. 1989). XRD patterns of the ferrihydrite samples heated to 220º C show minor sharpening of the broad peaks, but do not display discrete hematite peaks (data not shown). These data, together with the absence of the H_2O spectral feature at 1.90 μm, suggest that the ferrihydrite partially dehydrated and/or dehydroxylated toward nanophase hematite with heating under dry $N_{2(g)}$.

Thermal-IR emission spectra of untreated allophane and ferrihydrite have broad spectral bands resulting from poor crystallinity. The chemisorption of both sulfate and phosphate onto allophane results in the presence of shoulder features on the high frequency side of the Si-O stretching band from S-O and P-O bond vibrations, whereas sulfate and phosphate chemisorption on ferrihydrite causes an increase in the emissivity from ~1000-1250 cm^{-1} because of Christiansen features associated with S-O and P-O stretching vibrations (e.g., Christensen et al. 2000; Cloutis et al. 2006; Lane et al. 2008; Lane et al. 2015). Mineral abundances in rocks and soils can be estimated from TIR spectra with linear mixing algorithms using a library of mineral spectra collected in the laboratory (Ramsey and Christensen 1998). Small differences between library member spectra can affect which member is selected by the algorithm (e.g., Rampe et al. 2012). Inclusion of spectra for allophane and ferrihydrite with and without chemisorbed sulfate and phosphate anions in TES and mini-TES spectral libraries provides a way to model for the presence or absence of these materials on the martian surface. We suggest that these features would be more easily recognized in IR data from landers and rovers (e.g., mini-TES on MER) rather from orbiters because of the large footprint of orbital spectrometers and the ability of landed missions to target individual samples. However, we hypothesize that chemisorbed sulfate

550 and phosphate would be more difficult to recognize on high-silica allophane, as the Si-O
551 stretching band may interfere with the S-O and P-O stretching vibrations. The laboratory TIR
552 spectra of pressed pellets are relevant to npWP on the martian surface that are present as
553 cohesive coatings on larger grains. If the npWP on the martian surface are fine grained, then their
554 vibrational bands may be severely weakened by particle scattering (e.g., Salisbury and Wald
555 1992).

556 The presence of npWP on the martian surface has been previously inferred from orbital
557 TES data (Rampe et al. 2012) and CRISM data (Weitz et al. 2014), *in-situ* Mössbauer
558 spectroscopy (Morris et al. 2006a, 2006b, 2008), a combination of *in-situ* APXS chemical data
559 and Mössbauer spectroscopy (Clark et al. 2005; Ming et al. 2006), and *in-situ* TIR spectroscopy
560 by mini-TES (Ruff et al. 2011). MSL-CheMin XRD analyses confirm the presence of X-ray
561 amorphous phases in all martian rocks and soil samples measured to date and indicate that
562 amorphous phases are present in significant abundances (Bish et al. 2013; Vaniman et al. 2014;
563 Morris et al. 2015a). The amorphous backgrounds in XRD patterns of the Rocknest soil and the
564 Sheepbed mudstone appear to have one broad hump, rather than two as seen in allophane over
565 the CheMin angular range, which suggests that allophane is not a major phase in the amorphous
566 component. Additionally, the broad hump in CheMin data has a maximum near 30 degrees 2-
567 theta, which is inconsistent with the hump from ferrihydrite within the CheMin angular range
568 (~40 degrees 2-theta). MSL-SAM data from Rocknest and Sheepbed show broad low-T H_2O
569 releases, consistent with hydrated nanophase materials like allophane and ferrihydrite (Leshin et
570 al. 2014; Ming et al. 2014; Figure 9a). Furthermore, SAM m/z 18 data of the Sheepbed mudstone
571 have a shoulder near 275º C, consistent with allophane (Ming et al. 2014). However, calculations
572 of the composition of the crystalline and amorphous components using mineralogy from CheMin

573 and bulk chemistry from APXS show that the amorphous materials in Rocknest and Sheepbed
574 are relatively poor in Al_2O_3, so allophane would only be a minor phase if present at all (Dehouck
575 et al. 2014; Morris et al. 2015a). SAM data from Rocknest and Sheepbed show SO_2 evolutions
576 from ~450-800 ºC, where Rocknest data have two peak temperatures at ~500-550 ºC and ~700-
577 750 ºC (McAdam et al. 2014) and Sheepbed data have peak temperatures at 600-625 ºC with a
578 shoulder at ~675 ºC (Ming et al. 2014). Evolution of SO_2 from these samples is not consistent
579 with sulfate chemisorbed onto ferrihydrite or allophane (Figure 9b); however, SO_2 evolution
580 from other npWP may occur in this temperature range, and these investigations are ongoing.

581 Amorphous phases are ubiquitous on Mars, so it is important to take the chemisorption
582 properties of npWP into consideration when determining the speciation of S and P in rocks and
583 soils on the martian surface. We suggest using high-temperature EGA with the SAM instrument
584 to search for chemisorbed sulfate species in future samples measured at Gale crater, and the
585 magnitude of the m/z 64 releases can help quantify the abundances of adsorbed sulfate. The
586 shape of the amorphous background and the low-angle scattering intensity in CheMin patterns
587 can be used to help constrain the identification of the nanophase weathering products present.
588 The secondary mineralogy determined by CheMin may also be useful for estimating abundances
589 of adsorbed sulfate and phosphate. Previous studies have characterized sulfate and phosphate
590 adsorption isotherms with changing pH for many npWP (e.g., Arai and Sparks 2001; Jara et al.
591 2006; Antelo et al. 2010). The identification by CheMin of minerals that are diagnostic of pH
592 (e.g., jarosite, akaganeite) could help constrain pH and estimate the amount sulfate and
593 phosphate chemisorbed onto npWP and further improve our understanding of the physico-
594 chemical properties of amorphous material on Mars.

595 **Acknowledgements**

We gratefully acknowledge the Mars Space Flight Facility at Arizona State University for the use of their Thermal-IR spectroscopy laboratory; Alicia Rutledge for her help measuring TIR spectra; Charlie Galindo, Dean Muir, and Chris Carrier for measuring IC data; Roy Christofferson for TEM analyses; DC Golden for his expert advice on nanophase mineral syntheses and ion adsorption procedures; and Janice Bishop, Enver Murad, and an anonymous reviewer for their constructive comments on the manuscript. This work was funded by the NASA Mars Fundamental Research Program awarded to E.B. Rampe and R.V. Morris.

References Cited

Agresti, D. G., and Gerakines, P. A. (2009) Simultaneous fitting of Mars Mössbauer data. Hyperfine Interactions, 188, 113-120.

Agresti, D.G., Dyar, M.D., and Schaefer, M.W. (2006) Velocity scales for Mars Mössbauer data. Hyperfine Interactions, 170, 67-74.

Antelo, J., and 6 colleagues (2010) Analysis of phosphate adsorption onto ferrihydrite using the CD-MUSIC model. Journal of Colloid and Interface Science, 347, 112-119.

Arai, Y. and Sparks, D.L. (2001) ATR-FTIR spectroscopic investigation on phosphate adsorption mechanisms at the ferrihydrite-water interface. Journal of Colloid and Interface Science, 241, 317-326.

Archer, P.D. Jr., Ming, D.W., and Sutter, B. (2013) The effects of instrument parameters and sample properties on thermal decomposition: interpreting thermal analysis data from Mars. Planetary Science, 2:2.

Bibring, J.-P., and 42 colleagues (2004) OMEGA: Observatoire pour la Minéralogie, l'eau, les Glaces et l'Activité. In A. Wilson, Ed., Mars Express: The Scientific Payload, ESA Publications Division, Noordwijk, Netherlands, p. 37-49.

619 Bish, D.L., and 19 colleagues (2013) X-ray diffraction results from Mars Science Laboratory:
620 Mineralogy of Rocknest at Gale crater. Science, 341, doi:10.1126/science.1238932.
621 Bishop, J.L., and Murad, E. (2002) Spectroscopic and geochemical analyses of ferrihydrite from
622 springs in Iceland and applications to Mars. In J. L. Smellie, and M. G. Chapman, Eds.,
623 Volcano-Ice Interactions on Earth and Mars, Geological Society, London, Special
624 Publications, 202, 357-370.
625 Bishop, J.L., and 6 colleagues. (2013) Spectral and hydration properties of allophane and
626 imogolite. Clays and Clay Minerals, 61, 57-74.
627 Blake, D.F., and 21 colleagues (2012) Characterization and calibration of the CheMin
628 mineralogical instrument on Mars Science Laboratory. Space Science Reviews, 170, 341-
629 399.
630 Blake, D.F., and 45 colleagues (2013) Curiosity at Gale Crater, Mars: Characterization and
631 analysis of the Rocknest sand shadow. Science, 341, doi:10.1126/science.1239505.
632 Borchardt, G. (1989) Smectites. In J. B. Dixon, and S. B. Weed, Eds., Minerals in Soil
633 Environments, p.675-727. SSSA Book Series, Soil Science Society of America, Madison,
634 Wisconsin.
635 Catling, D.C., and Moore, J.M. (2003) The nature of coarse-grained crystalline hematite and its
636 implication for the early environment of Mars. Icarus, 165, 277-300.
637 Cichota, R., Vogeler, I., Bolan, N.S., and Clothier, B.E. (2007) Simultaneous adsorption of
638 calcium and sulfate and its effect on their movement. Soil Science Society of America
639 Journal, 71, 703-710.
640 Chevrier, V., Rochette, P., Mathé, P.-E., and Grauby, O. (2004) Weathering of iron-rich phases
641 in simulated Martian atmospheres. Geology, 32, 1033-1036.

642 Christensen, P.R., and Harrison, S.T. (1993) Thermal infrared emission spectroscopy of natural
643 surfaces: Application to desert varnish coatings on rocks. Journal of Geophysical Research,
644 98, 19,819-19,834.
645 Christensen, P.R., and 7 colleagues (2000) A thermal emission spectral library of rock-forming
646 minerals. Journal of Geophysical Research, 105, 9735-9739.
647 Clark, B., and 23 colleagues. (2005) Chemistry and mineralogy of outcrops at Meridiani Planum.
648 Earth and Planetary Science Letters, 240, 73-94.
649 Cloutis, E.A., and 11 colleagues. (2006) Detection and discrimination of sulfate minerals using
650 reflectance spectroscopy. Icarus, 184, 121-157.
651 Conel, J. (1969) Infrared emissivities of silicates: Experimental results and a cloudy atmosphere
652 model of spectral emission from condensed particulate mediums. Journal of Geophysical
653 Research, 74, 1614-1634.
654 Dehouck, E., McLennan, S.M., Meslin, P.-Y., and Cousin, A. (2014) Constraints on abundance,
655 composition, and nature of X-ray amorphous components of soils and rocks at Gale crater,
656 Mars. Journal of Geophysical Research, 119, doi:10.1002/2014JE004716.
657 Elsheikh, M. A., Matsue, N., and Henmi, T. (2009) Effect of Si/Al ratio of allophane on
658 competitive adsorption of phosphate and oxalate. International Journal of Soil Science, 4, 1-
659 13.
660 Farmer, V.C., Ed. (1974) The Infrared Spectra of Minerals, 539 p., Mineralogical Society,
661 London.
662 Frost, R.L., Mills, S.J., Erickson, K.L. (2004) Thermal decomposition of peisleyite: a
663 thermogravimetry and hot stage Raman spectroscopic study. Thermochimica Acta, 419,
664 109-114.

665 Gallini, S., Jurado, J.R., and Colomer, M.T. (2005) Synthesis and characterization of monazite-
666 type Sr:LaPO4 prepared through coprecipitation. Journal of the European Ceramic Society,
667 25, 2003-2007.
668 Gálvez, N., Barrón, V., and Torrent, J. (1999) Effect of phosphate on the crystallization of
669 hematite, goethite, and lepidocrocite from ferrihydrite. Clays and Clay Minerals, 47, 304-
670 311.
671 Hoffman, J.H., Chaney, R.C., and Hammack, H. (2008) Phoenix Mars Mission – The Thermal
672 Evolved Gas Analyzer. Journal of the American Society for Mass Spectrometry, 19, 1377-
673 1383.
674 Hunt, G.R., Salisbury, J.W., and Lenhoff, C.J. (1971) Visible and near-infrared spectra of
675 minerals and rocks: IV. Sulphides and sulphates. Modern Geology, 3, 1-14.
676 Ishiguro, M., Makino, T., and Hattori, Y. (2006) Sulfate adsorption and surface precipitation on a
677 volcanic ash soil (allophanic andisol). Journal of Colloid and Interface Science, 300, 504-
678 510.
679 Janney, D.E., Cowley, J.M., and Busek, P.R. (2000) Transmission electron microscopy of
680 synthetic 2- and 6-line ferrihydrite. Clays and Clay Minerals, 48, 111-119.
681 Jara, A.A., Violante, A., Pigna, M., and de la Luz Mora, M. (2006) Mutual interactions of
682 sulfate, oxalate, citrate, and phosphate on synthetic and natural allophanes. Soil Science
683 Society of America Journal, 70, 337-346.
684 Khare, N., Martin, J.D., and Hesterberg, D. (2007) Phosphate bonding configuration on
685 ferrihydrite based on molecular orbital calculations and XANES fingerprinting. Geochimica
686 et Cosmochimica Acta, 71, 4405-4415.

687 Klingelhöfer, G., and 14 colleagues (2003) Athena MIMOS II Moessbauer spectrometer
688 investigation. Journal of Geophysical Research, 108, 8067, doi:8010.1029/2003JE002138.
689 Kwon, K.D., and Kubicki, J.D. (2004) Molecular orbital theory study on surface complex
690 structures of phosphates to iron hydroxides: Calculation of vibrational frequencies and
691 adsorption energies. Langmuir, 20, 9249-9254.
692 Lane, M.D., Bishop, J.L., Dyar, M.D., King, P.L., Parente, M., and Hyde, B.C. (2008)
693 Mineralogy of the Paso Robles soils on Mars. American Mineralogist, 93, 728-739.
694 Lane, M.D., and 7 colleagues (2015) Mid-infrared emission spectroscopy and visible/near-
695 infrared reflectance spectroscopy of Fe-sulfate minerals. American Mineralogist, 100, 66-82.
696 Leshin, L.A., and 34 colleagues (2014) Volatile, isotope, and organic analysis of martian fines
697 with the Mars Curiosity rover. Science, 341, doi:10.1126/science.1238937.
698 Lombardi, G. (1984) Thermal analysis in the investigation of zeolitized and altered volcanics of
699 Latium, Italy. Clay Minerals, 19, 789-801.
700 Mahaffy, P.R., and 84 colleagues. (2012) The Sample Analysis at Mars investigation and
701 instrument suite. Space Science Reviews, 170, 401-478.
702 Martín-Torres, F.J., and 24 colleagues (2015) Transient liquid water and water activity at Gale
703 crater on Mars. Nature Geoscience, 8, 357-361.
704 McAdam, A.C., and 24 colleagues (2014) Sulfur-bearing phases detected by evolved gas
705 analysis of the Rocknest aeolian deposit, Gale Crater, Mars. Journal of Geophysical
706 Research, 119, 373-393.
707 McAdam, A.C., and 17 colleagues (2015) Major volatiles from MSL SAM evolved gas analyses:
708 Yellowknife Bay through lower Mount Sharp. 46th Lunar and Planetary Science Conference,
709 Abstract 2323.

Michalski, J.R., Kraft, M.D., Sharp, T.G., Williams, L.B., and Christensen, P.R. (2005) Mineralogical constraints on the high-silica martian surface component observed by TES. Icarus, 174, 161-177.

Ming, D.W., and 16 colleagues (2006) Geochemical and mineralogical indicators for aqueous processes in the Columbia Hills of Gusev crater, Mars. Journal of Geophysical Research, 111, doi:10.1029/2005JE002560.

Ming, D.W., and 57 colleagues (2014) Volatile and organic compositions of sedimentary rocks in Yellowknife Bay, Gale Crater, Mars. Science, 343, doi:10.1126/science.1245267.

Morris, R.V., Agresti, D.G., Lauer, H.V., Jr., Newcomb, J.A., Shelfer, T.D., and Murali, A.V. (1989) Evidence for pigmentary hematite on Mars based on optical, magnetic, and Mössbauer studies of superparamagnetic (nanocrystalline) hematite. J. Geophys. Res., 94, 2760-2778.

Morris, R.V., Golden, D.C., Bell, J.F. III, Lauer, H.V. Jr., and Adams, J.B. (1993) Pigmenting agents in Martian soils: Inferences from spectral, Mössbauer, and magnetic properties of nanophase and other iron oxides in Hawaiian palagonitic soil PN-9. Geochimica et Cosmochimica Acta, 57, 4597-4609.

Morris, R.V., and 11 colleagues (2000), Mineralogy, composition, and alteration of Mars Pathfinder rocks and soils: Evidence from multispectral, elemental, and magnetic data on terrestrial analogue, SNC meteorite, and Pathfinder samples, Journal of Geophysical Research, 105, 1757-1817, doi:10.1029/1999JE001059.

Morris, R.V., and 7 colleagues (2001) Phyllosilicate-poor palagonitic dust from Mauna Kea Volcano (Hawaii): A mineralogical analogue for magnetic Martian dust? Journal of Geophysical Research, 106, 5057-5083.

Morris, R.V., and 19 colleagues (2006a), M□ssbauer mineralogy of rock, soil and dust at Gusev crater, Mars: Spirit's journey through weakly altered olivine basalt on the plains and pervasively altered basalt in the Columbia Hills, Journal of Geophysical Research, 111, doi:10.1029/2005JE002584.

Morris, R.V., and 23 colleagues (2006b), M□ssbauer mineralogy of rock, soil, and dust at Meridiani Planum, Mars: Opportunity's journey across sulfate-rich outcrop, basaltic sand and dust, and hematite lag deposits, Journal of Geophysical Research, 111, doi:10.1029.2006JE02791.

Morris, R.V., and 16 colleagues (2008) Iron mineralogy and aqueous alteration from Husband Hill through Home Plate at Gusev Crater, Mars: Results from the Mössbauer instrument on the Spirit Mars Exploration Rover. Journal of Geophysical Research, 113, doi:10.1029/2008JE003201.

Morris, R.V., and 24 colleagues (2015a) Update on the Chemical composition of crystalline, smectite, and amorphous components for Rocknest soil and John Klein and Cumberland mudstone drill fines at Gale crater, Mars. LPS XLVI, 2622.

Morris, R.V., and 6 colleagues (2015b) Transmission X-ray diffraction (XRD) patterns relevant to the MSL CheMin amorphous component: Sulfates and silicates. LPS XLVI 2434.

Murchie, S., and 49 colleagues (2007) Compact Reconnaissance Imaging Spectrometer for Mars (CRISM) on Mars Reconnaissance Orbiter (MRO). Journal of Geophysical Research, 112, doi:10.1029/2006JE002682.

Nanzyo, M., Dahlgren, R., and Shoji, S. (1993) Chemical characteristics of volcanic ash soils. In Shoji, S., Nanzyo, M., and Dahlgren, R., Eds., Volcanic Ash Soils: Genesis, Properties and Utilization, p.145-188 Developments in Soil Science, Elsevier, Amsterdam.

Ohashi, F., Wada, S.-I., Suzuki, M., Maeda, M., and Tomura, S. (2002) Synthetic allophane from high-concentration solutions: nanoengineering of the porous solid. Clay Minerals, 37, 451-456.

Parfitt, R. L. (1990) Allophane in New Zealand – A review. Australian Journal of Soil Research, 28, 343-360.

Parfitt, R.L., and Hemni, T. (1980) Structure of some allophanes from New Zealand. Clays and Clay Minerals, 28, 285-294.

Pollard, R. J., Cardile, C. M., Lewis, D. G., and Brown, L. J. (1992) Characterization of FeOOH polymorphs and ferrihydrite using low-temperature, applied-field, Mossbauer spectroscopy. Clays and Clay Minerals, 27, 57-71.

Rajan, S.S.S. (1979) Adsorption and desorption of sulfate and charge relationships in allophanic clays. Soil Science Society of America Journal, 43, 65-69.

Rampe, E.B., Kraft, M.D., Sharp, T.G., Golden, D.C., Ming, D.W., and Christensen, P.R. (2012) Allophane detection on Mars with Thermal Emission Spectrometer data and implications for regional-scale chemical weathering processes. Geology, 40, 995-998.

Ramsey, M.S., and Christensen, P.R. (1998) Mineral abundance determination: Quantitative deconvolution of thermal emission spectra. Journal of Geophysical Research, 103, 577-596.

Ruff, S.W., Christensen, P.R., Barbera, P.W., and Anderson, D.L. (1997) Quantitative thermal emission spectroscopy of minerals: A laboratory technique for measurement and calibration. Journal of Geophysical Research, 102, 14,899-14,913.

Ruff, S.W., and 10 colleagues (2011) Characteristics, distribution, origin, and significance of opaline silica observed by the Spirit rover in Gusev crater, Mars. Journal of Geophysical Research, 116, doi:10.1029/2010JE003767.

779 Salisbury, J.W., and Wald, A. (1992) The role of volume scattering in reducing spectral contrast
780 of reststrahlen bands in spectra of powdered minerals. Icarus, 96, 121-128.
781 Schwertmann, U., and Taylor, R.M. (1989) Iron oxides. In J. B. Dixon, and S. B. Weed, Eds.,
782 Minerals in Soil Environments, p. 379-438. SSSA Book Series, Soil Science Society of
783 America, Madison, Wisconsin.
784 Schwertmann, U., and Cornell, R.M. (2000) Iron Oxides in the Laboratory: Preparation and
785 Characterization, 188 p. Wiley-VCH, Weinheim, Germany.
786 Stern, J.C., and 11 colleagues (2013) Isotopic and geochemical investigation of two distinct Mars
787 analog environments using evolved gas techniques in Svalbard, Norway. Icarus, 224, 297-
788 308.
789 Su, C., and Harsh, J.B. (1993) The electrophoretic mobility of imogolite and allophane in the
790 presence of inorganic anions and citrate. Clays and Clay Minerals, 41, 461-471.
791 Šubrt, J., Štengl, V., and Skokánek, M. (1992) Decomposition of ferrihydrite prepared from
792 $Fe(NO_3)_3$ aqueous solutions under varying pH. Thermochimica Acta, 211, 107-119.
793 van der Gaast, S.J., Wada, K., Wada, S.-I., and Kakuto, Y. (1985) Small-angle X-ray powder
794 diffraction, morphology, and structure of allophane and imogolite. Clays and Clay Minerals,
795 33, 237-243.
796 Vaniman, D.T., and 36 colleagues (2014) Mineralogy of a mudstone at Yellowknife Bay, Gale
797 Crater, Mars. Science, 343, doi:10.1126/science.1243480.
798 Vempati, R.K., Loeppert, R.H., Sittertz-Bhatkar, H., and Burghardt, R.C. (1990) Infrared
799 vibrations of hematite formed from aqueous- and dry-thermal incubation of Si-containing
800 ferrihydrite. Clays and Clay Minerals, 38, 294-298.

Wada, K. (1987) Minerals formed and mineral formation from volcanic ash by weathering. Chemical Geology, 60, 17-28.

Wada, K. (1989) Allophane and Imogolite. In J. B. Dixon, and S. B. Weed, Eds., Minerals in Soil Environments, p.1051-1087. SSSA Book Series, Soil Science Society of America, Madison, Wisconsin.

Wada, S.-I., Eto, A., and Wada, K. (1979) Synthetic allophane and imogolite. The Journal of Soil Science, 30, 347-355.

Weitz, C. M., Bishop, J. L., Baker, L. L., and Berman, D. C. (2014) Fresh exposures of hydrous Fe-bearing amorphous silicates on Mars. Geophysical Research Letters, 41, 8744-8751.

Willett, I.R., Chartress, C.J., and Nguyen, T.T. (1988) Migration of phosphate into aggregated particles of ferrihydrite. Journal of Soil Science, 39, 275-282.

Zhu, M., Northrup, P., Chenyang, S., Billinge, S.J.L., Sparks, D.L., and Waychunas, G.A. (2014) Structure of sulfate adsorption complexes on ferrihydrite, Environmental Science and Technology Letters, 1, 97-101.

Figure Captions

Figure 1. Reactions demonstrating specific adsorption of sulfate on the Al-OH surface of allophane and the formation of different types of sulfate ligands: (**a**) deprotonated monodentate mononuclear, (**b**) deprotonated bidentate binuclear, and (**c**) diprotonated bidentate binuclear. Note that all reactions result in the removal of H_2O. Figure is after Ishiguro et al. (2006) and Kwon and Kubicki (2004).

Figure 2. (**a-c**) Transmission electron microscopy (TEM) of phosphate-chemisorbed allophane: (**a**) TEM image of allophane cluster, (**b**) Selected area electron diffraction (SAED) of allophane, and (**c**) high-resolution TEM image of allophane. (**d-f**) Transmission electron microscopy of phosphate-chemisorbed ferrihydrite: (**d**) TEM image of ferrihydrite cluster, (**e**) SAED of ferrihydrite, and (**f**) high-resolution TEM image of ferrihydrite with small areas of lattice fringes denoted by black arrows. Results of TEM of sulfate-chemisorbed npWP samples are similar.

Figure 3. X-ray diffraction patterns of (**a**) untreated, phosphate-chemisorbed, and sulfate-chemisorbed allophane, and (**b**) untreated, phosphate-chemisorbed, and sulfate-chemisorbed ferrihydrite. Allophane samples were measured under Cu-Kα radiation, and the patterns were calculated for Co-Kα.

Figure 4. Evolved gas analysis data of (**a**) m/z 18 ($H_2O_{(g)}$) and m/z 64 ($SO_{2(g)}$) measured from untreated, sulfate-chemisorbed, and phosphate-chemisorbed allophane, and (**b**) m/z 18 ($H_2O_{(g)}$) and m/z 64 ($SO_{2(g)}$) measured from untreated, sulfate-chemisorbed, and phosphate-chemisorbed ferrihydrite. Samples were measured under Sample Analysis at Mars-like operating conditions.

Figure 5. Three-doublet fit for Mössbauer spectra of sulfate-chemisorbed 2-line ferrihydrite equilibrated (**a**) in lab air and (**b**) at 220 ºC under desiccating conditions (dry $N_{2(g)}$). TC = total counts; BC = baseline counts.

847 **Figure 6.** (**a**) Visible/near-infrared reflectance spectra of untreated, sulfate-chemisorbed, and
848 phosphate-chemisorbed allophane measured under ambient conditions and in a N_2(g)-purged
849 glove box at 25, 110, and 220º C. Dashed vertical lines are at 1.38 μm, 1.91 μm, and 2.20 μm.
850 Spectra are offset for clarity. (**b**) Visible/near-IR reflectance spectra of untreated, sulfate-
851 chemisorbed, and phosphate-chemisorbed ferrihydrite measured under the same conditions as the
852 allophane spectra. Dashed vertical lines are at 1.40 μm, 1.91 μm, and 2.30 μm. Spectra have
853 been continuum removed and are offset for clarity.
854 **Figure 7.** Thermal infrared emission spectra of (**a**) untreated, sulfate-chemisorbed, and
855 phosphate-chemisorbed allophane, and (**b**) untreated, sulfate-chemisorbed, and phosphate-
856 chemisorbed ferrihydrite.
857 **Figure 8.** Laboratory Visible/near-infrared spectra of untreated and chemisorbed ferrihydrite
858 measured at room temperature and lab air and under $N_{2(g)}$ at room temperature, 110º C, and 220º
859 C. Dashed vertical lines are at 630 and 860 nm. Spectra are offset for clarity.
860 **Figure 9.** Evolved das analysis data of (**a**) m/z 19 ($H_2O_{(g)}$) measured from Rocknest (RN) and
861 John Klein (JK) samples by SAM and m/z 18 ($H_2O_{(g)}$) measured from npWP in the laboratory,
862 and (**b**) m/z 66 ($SO_{2(g)}$) measured from Rocknest (RN) and John Klein (JK) samples by SAM and
863 m/z 64 ($SO_{2(g)}$) measured from npWP in the laboratory. Traces from m/z 19 and 66 are displayed
864 for Sample Analysis at Mars data because the detector was saturated for m/z 18 and 64. Runs 2
865 and 4 are displayed for RN and JK, respectively.
866
867
868
869

870 **Tables**

Table 1. Mössbauer parameters (room temperature) calculated from least squares fitting procedure for one- and three-doublet models for 2-line ferrihydrite without adsorbed anions and with adsorbed sulfate and phosphate anions.

	Ambient			Desiccated 220°C		
Adsorbed Anion	None	Sulfate	Phosphate	None	Sulfate	Phosphate
One doublet model						
CS (mm/s)	0.35(2)	0.34(2)	0.34(2)	0.34(2)	0.34(2)	0.34(2)
QS (mm/s)	0.73(2)	0.72(2)	0.74(2)	0.75(2)	0.75(2)	0.81(2)
FWHM (mm/s)	0.51(2)	0.52(2)	0.55(2)	0.54(2)	0.56(2)	0.57(2)
A (%)	100	100	100	100	100	100
Three doublet model						
Ferric doublet 1						
CS (mm/s)	0.34(2)	0.34(2)	0.34(2)	0.34(2)	0.34(2)	0.34(2)
QS (mm/s)	0.45(2)	0.45(2)	0.43(2)	0.53(2)	0.50(2)	0.56(2)
FWHM (mm/s)	0.36(2)	0.38(2)	0.37(2)	0.40(2)	0.41(2)	0.41(2)
A (%)	36(4)	40(5)	33(6)	53(4)	42(5)	51(2)
Ferric doublet 2						
CS (mm/s)	0.34(2)	0.34(2)	0.34(2)	0.33(2)	0.34(2)	0.34(2)
QS (mm/s)	0.78(2)	0.78(2)	0.77(2)	0.91(2)	0.84(2)	0.96(2)
FWHM (mm/s)	0.33(2)	0.34(3)	0.36(3)	0.35(2)	0.39(2)	0.35(2)
A (%)	38(6)	36(8)	38(9)	31(6)	34(8)	31(3)
Ferric doublet 3						
CS (mm/s)	0.34(2)	0.33(2)	0.33(2)	0.32(2)	0.32(2)	0.32(2)
QS (mm/s)	1.17(2)	1.17(2)	1.18(2)	1.31(2)	1.22(2)	1.39(2)
FWHM (mm/s)	0.38(2)	0.39(2)	0.44(2)	0.38(2)	0.45(2)	0.39(2)
A (%)	24(3)	24(4)	29(4)	16(2)	24(4)	18(2)

CS = center shift relative to metallic iron foil at room temperature; QS = quadrupole splitting; FWHM = full width at half maximum intensity. A = subspectral area. Uncertainty of the final digit given in parenthesis.

871

872

873

874

875

876

877

878

879

880 **Table 2.** Band minima of allophane samples determined from corrected reflectance spectra.

Sample	1.4 μm band minimum	1.9 μm band minimum
	25 ºC – Lab Air	
Untreated	1.413	1.939
Chemisorbed-SO_4	1.406	1.929
Chemisorbed-PO_4	1.406	1.918
	25 ºC – $N_{2(g)}$	
Untreated	1.413	1.939
Chemisorbed-SO_4	1.406	1.929
Chemisorbed-PO_4	1.406	1.918
	110 ºC – $N_{2(g)}$	
Untreated	1.400	1.936
Chemisorbed-SO_4	1.389	1.921
Chemisorbed-PO_4	1.381	1.916
	220 ºC – $N_{2(g)}$	
Untreated	1.378	1.929
Chemisorbed-SO_4	1.382	1.921
Chemisorbed-PO_4	1.380	1.921

881

Figure 1

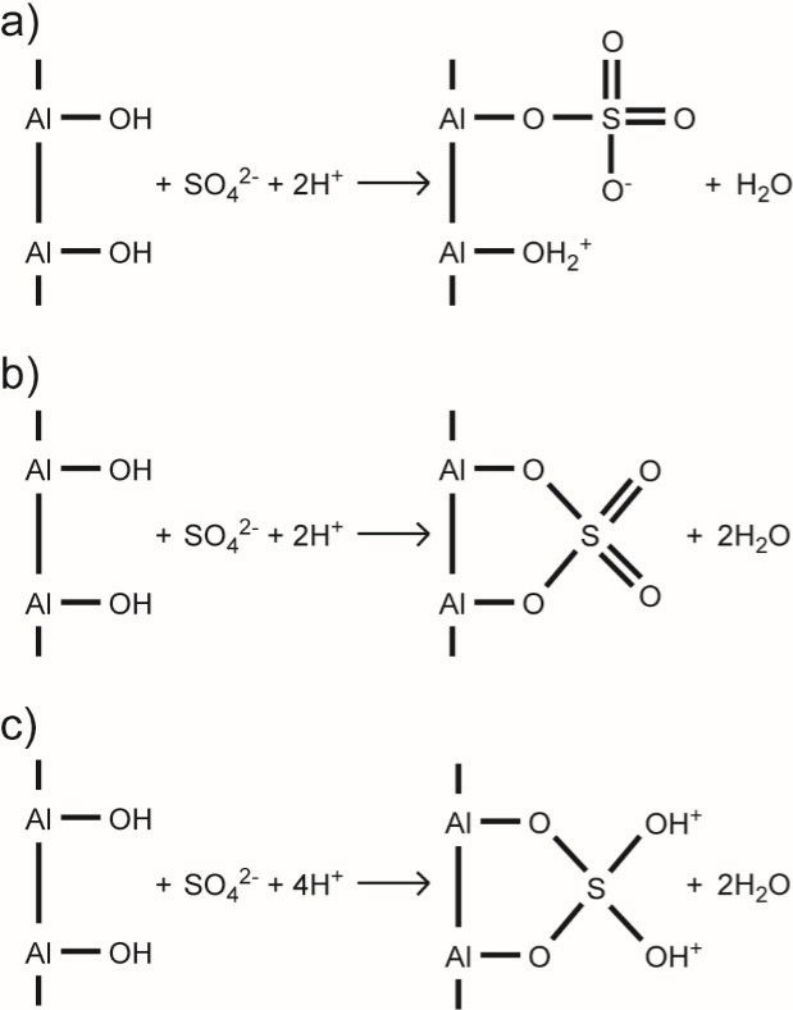
a)
Al — OH
Al — OH
+ SO_4^{2-} + $2H^+$
Al — O — S(=O)(=O)(=O)$^-$
Al — OH_2^+
+ H_2O
b)
Al — OH
Al — OH
+ SO_4^{2-} + $2H^+$
Al — O
Al — O
S(=O)(=O)
+ $2H_2O$
c)
Al — OH
Al — OH
+ SO_4^{2-} + $4H^+$
Al — O
Al — O
S
OH^+
OH^+
+ $2H_2O$

Figure 2

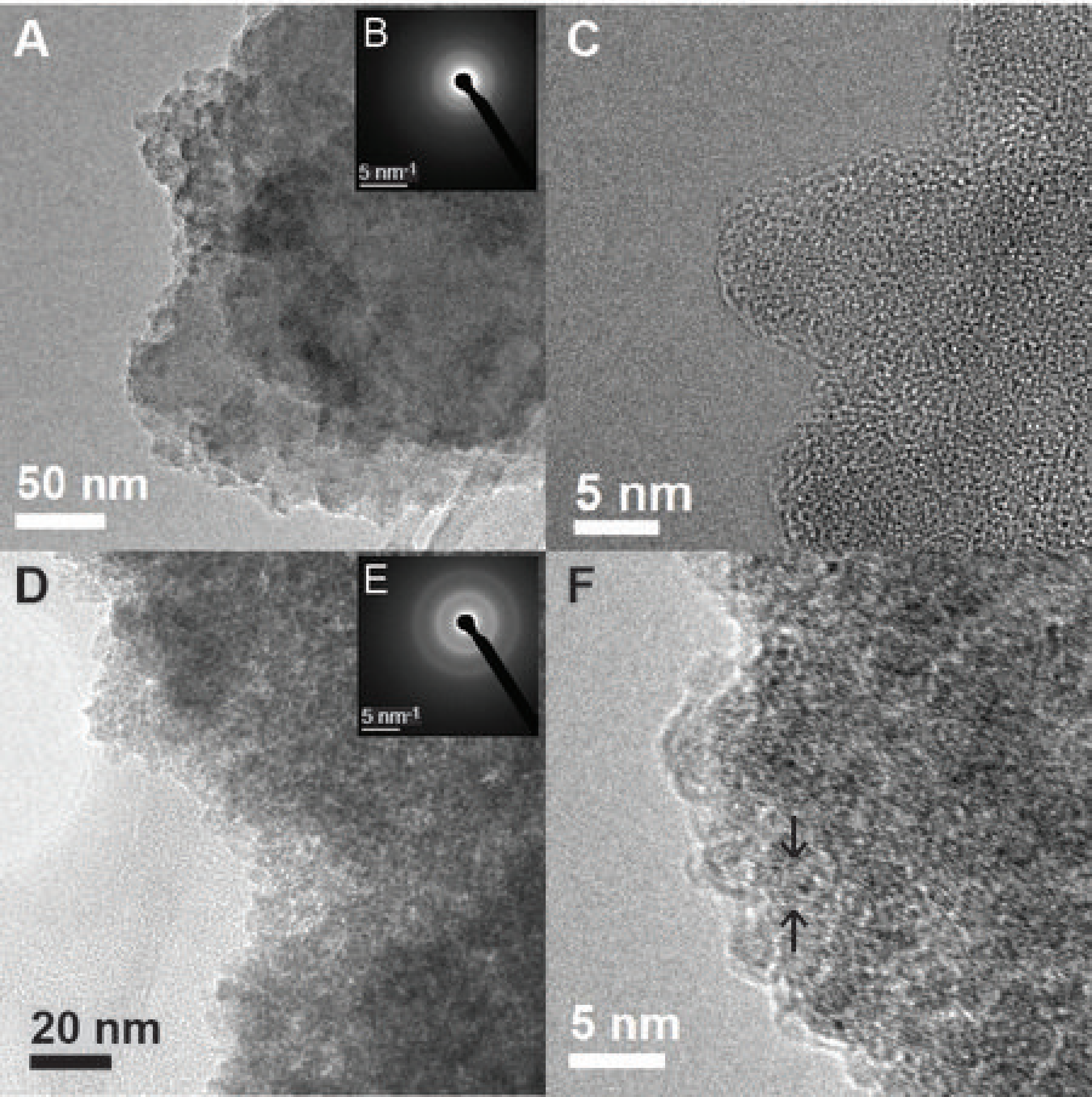

Figure 3

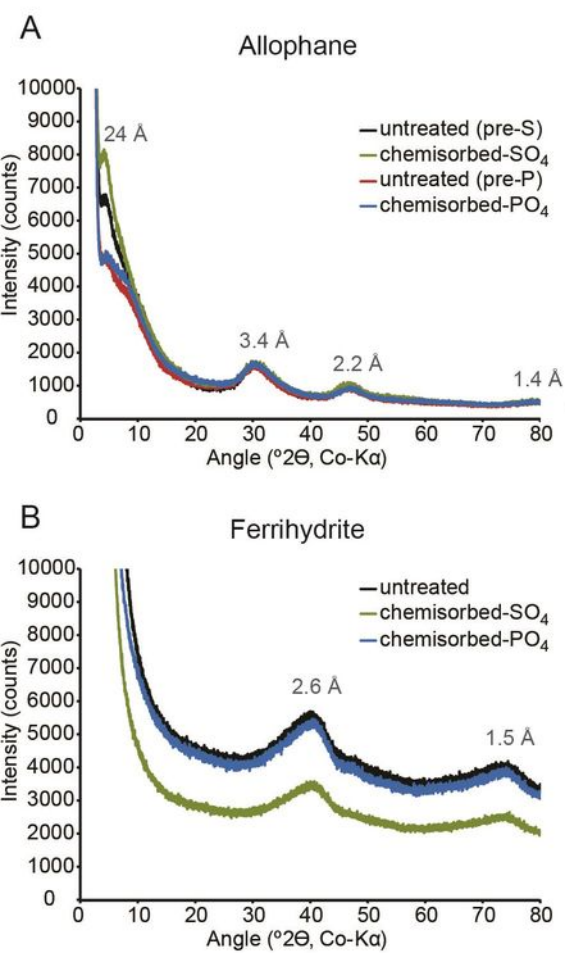
A
Allophane
24 Å
3.4 Å
2.2 Å
1.4 Å
untreated (pre-S)
chemisorbed-SO4
untreated (pre-P)
chemisorbed-PO4
Intensity (counts)
Angle (°2Θ, Co-Kα)
B
Ferrihydrite
2.6 Å
1.5 Å
untreated
chemisorbed-SO4
chemisorbed-PO4
Intensity (counts)
Angle (°2Θ, Co-Kα)

Figure 4

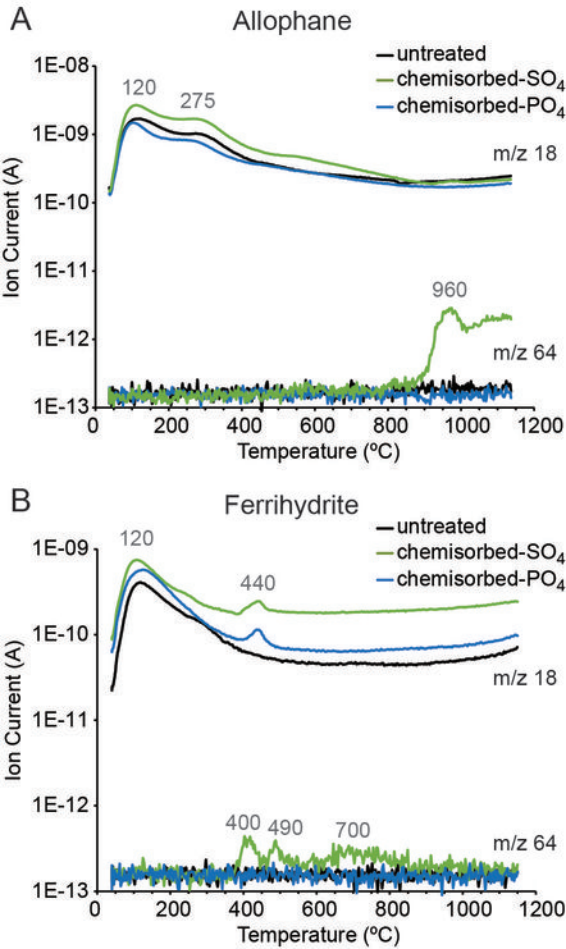
A
Allophane
untreated
chemisorbed-SO4
chemisorbed-PO4
120
275
960
m/z 18
m/z 64
Ion Current (A)
1E-08
1E-09
1E-10
1E-11
1E-12
1E-13
0
200
400
600
800
1000
1200
Temperature (ºC)
B
Ferrihydrite
untreated
chemisorbed-SO4
chemisorbed-PO4
120
440
400
490
700
m/z 18
m/z 64
Ion Current (A)
1E-09
1E-10
1E-11
1E-12
1E-13
0
200
400
600
800
1000
1200
Temperature (ºC)

Figure 5

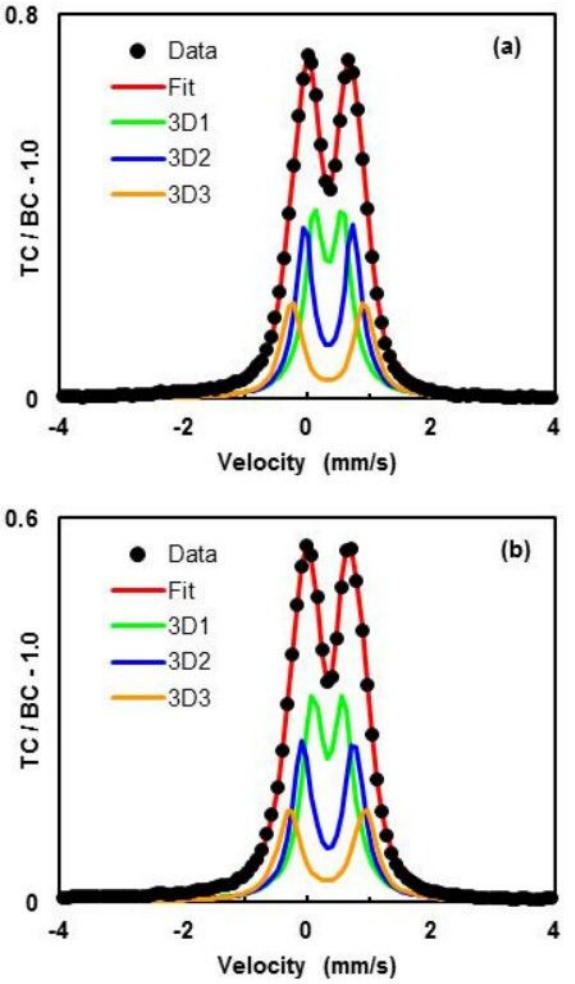
0.8
Data
Fit
3D1
3D2
3D3
(a)
TC / BC - 1.0
0
-4
-2
0
2
4
Velocity (mm/s)
0.6
Data
Fit
3D1
3D2
3D3
(b)
TC / BC - 1.0
0
-4
-2
0
2
4
Velocity (mm/s)

Figure 6

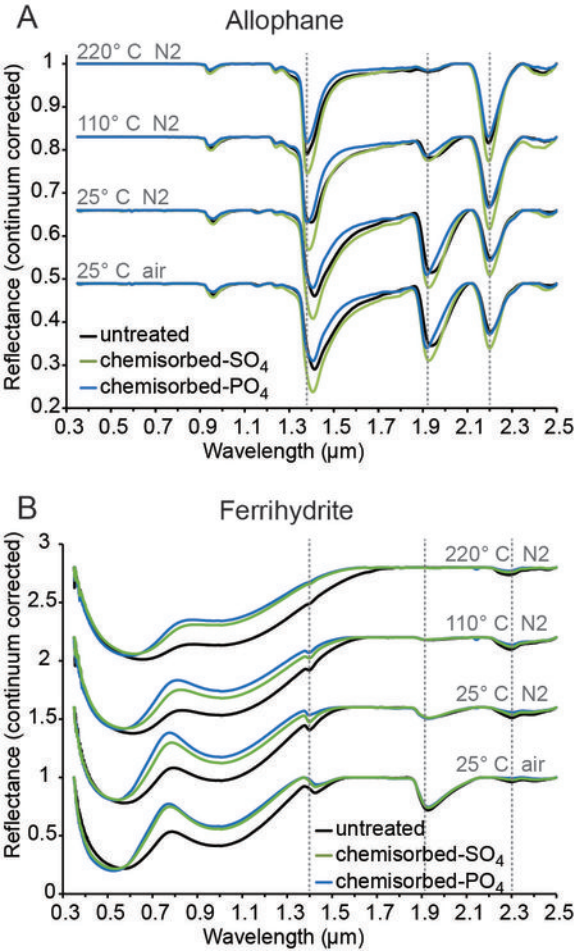
A
Allophane
220° C N2
110° C N2
25° C N2
25° C air
untreated
chemisorbed-SO4
chemisorbed-PO4
Reflectance (continuum corrected)
Wavelength (μm)
B
Ferrihydrite
220° C N2
110° C N2
25° C N2
25° C air
untreated
chemisorbed-SO4
chemisorbed-PO4
Reflectance (continuum corrected)
Wavelength (μm)

Figure 7

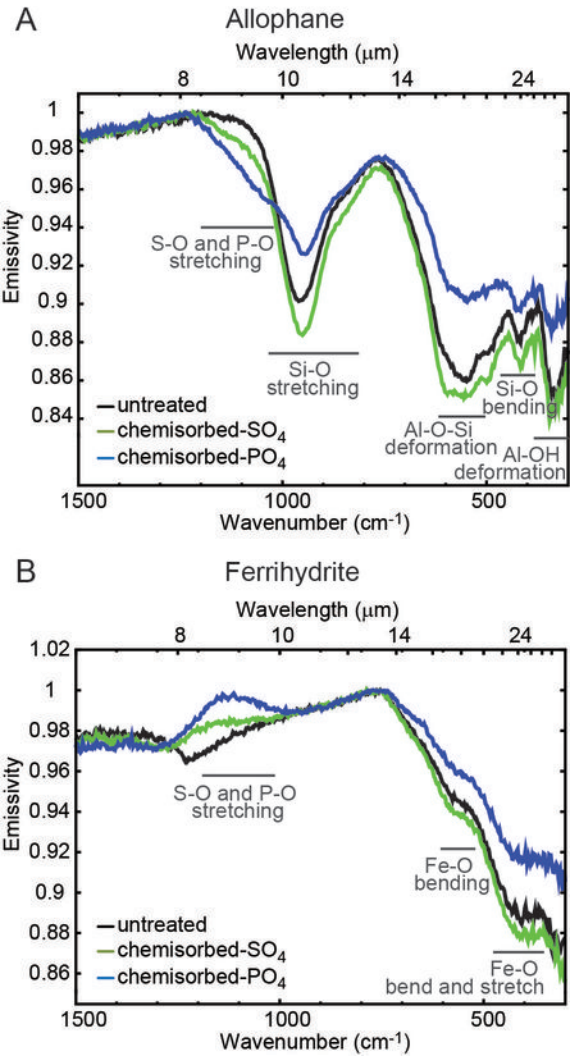
A
Allophane
Wavelength (μm)
8
10
14
24
1
0.98
0.96
0.94
0.92
0.9
0.88
0.86
0.84
Emissivity
S-O and P-O stretching
Si-O stretching
Si-O bending
Al-O-Si deformation
Al-OH deformation
untreated
chemisorbed-SO4
chemisorbed-PO4
1500
1000
500
Wavenumber (cm-1)
B
Ferrihydrite
Wavelength (μm)
8
10
14
24
1.02
1
0.98
0.96
0.94
0.92
0.9
0.88
0.86
Emissivity
S-O and P-O stretching
Fe-O bending
Fe-O bend and stretch
untreated
chemisorbed-SO4
chemisorbed-PO4
1500
1000
500
Wavenumber (cm-1)

Figure 8

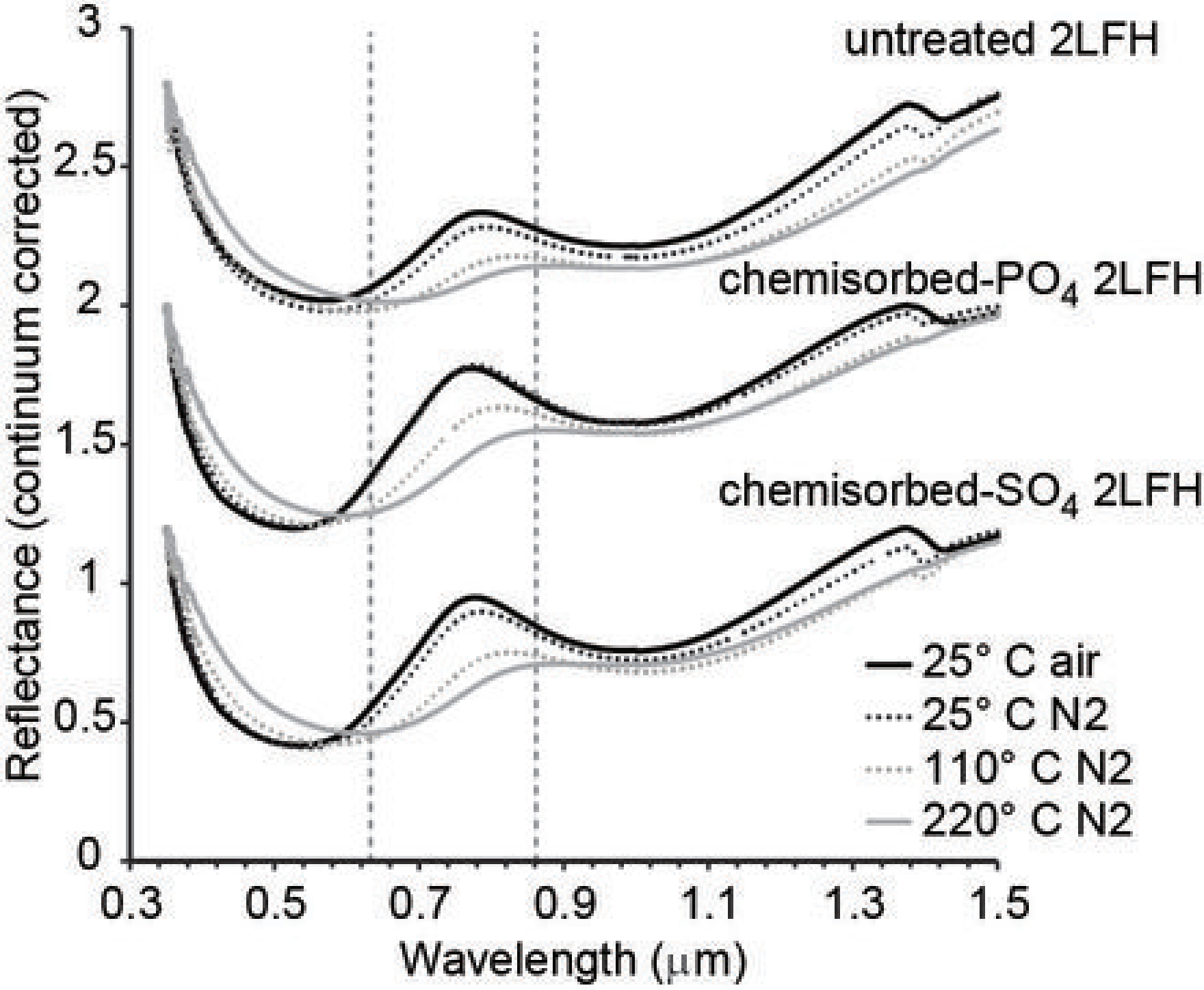
untreated 2LFH
chemisorbed-PO4 2LFH
chemisorbed-SO4 2LFH
25° C air
25° C N2
110° C N2
220° C N2
Reflectance (continuum corrected)
Wavelength (μm)
0
0.5
1
1.5
2
2.5
3
0.3
0.5
0.7
0.9
1.1
1.3
1.5

Figure 9

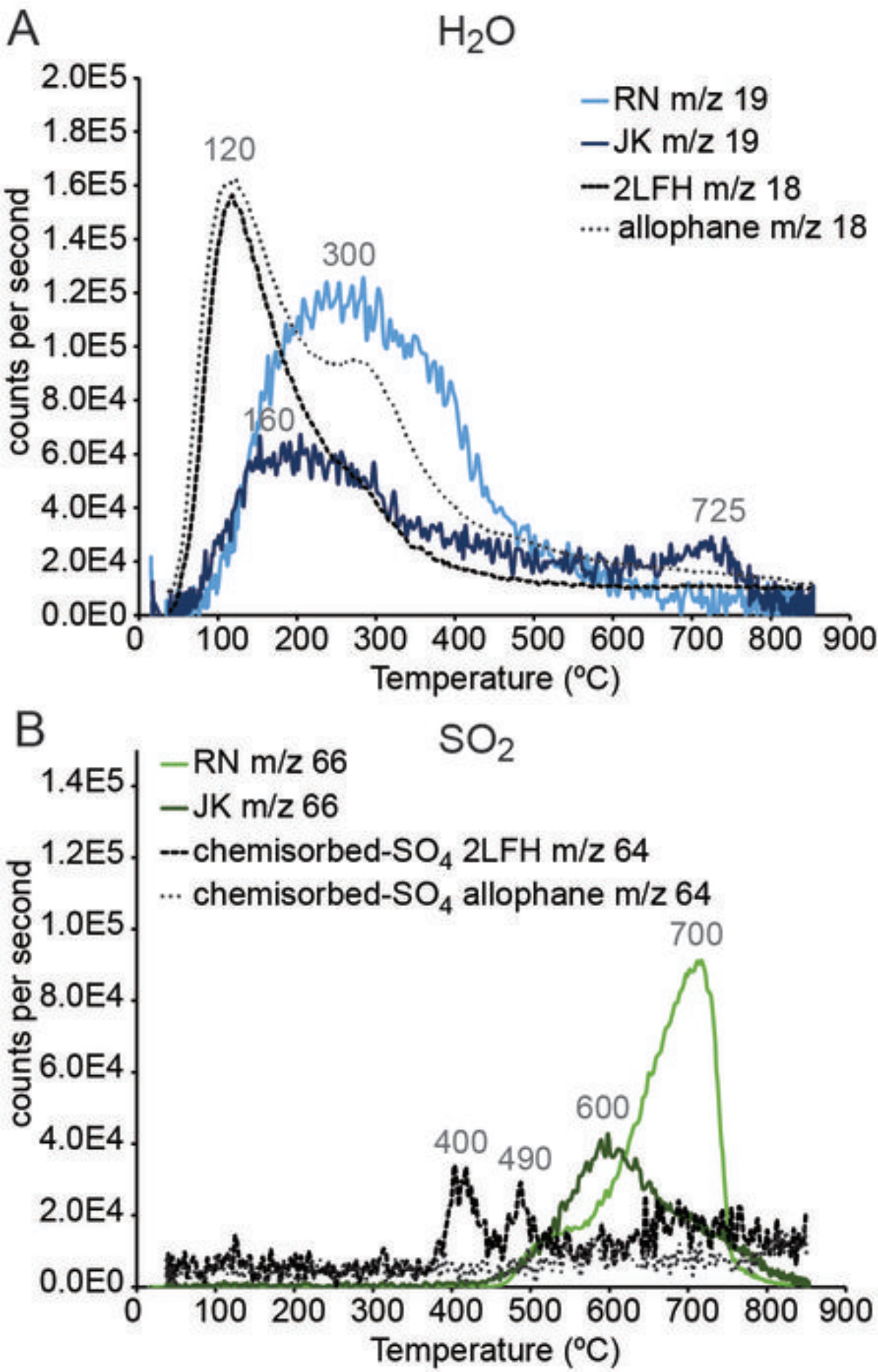
A
H_2O
RN m/z 19
JK m/z 19
2LFH m/z 18
allophane m/z 18
120
300
160
725
counts per second
2.0E5
1.8E5
1.6E5
1.4E5
1.2E5
1.0E5
8.0E4
6.0E4
4.0E4
2.0E4
0.0E0
0
100
200
300
400
500
600
700
800
900
Temperature (ºC)
B
SO_2
RN m/z 66
JK m/z 66
chemisorbed-SO_4 2LFH m/z 64
chemisorbed-SO_4 allophane m/z 64
700
600
400
490
counts per second
1.4E5
1.2E5
1.0E5
8.0E4
6.0E4
4.0E4
2.0E4
0.0E0
0
100
200
300
400
500
600
700
800
900
Temperature (ºC)